Fe-coverage-induced out-of-plane spin components of the antiferromagnetic spin structure in exchange-biased Fe/$FeSn_2$ bilayers

F. Stromberg and W. Keune*
Fachbereich Physik, Universität Duisburg-Essen (Campus Duisburg), D-47048, Duisburg, Germany

V. E. Kuncser
National Institute of Materials Physics, P.O.Box MG 7, 77125, Bucharest-Magurele, Romania

K. Westerholt
Institut für Experimentalphysik, Ruhr-Universität Bochum, D-44780 Bochum, Germany
(Received 28 December 2004; revised manuscript received 20 May 2005; published 19 August 2005)

Exchange-coupled Fe/$FeSn_2$(001) bilayer systems consisting of a polycrystalline ferromagnetic Fe layer grown on an epitaxial antiferromagnetic $FeSn_2$ layer have been prepared by molecular beam epitaxy and investigated by ^{57}Fe conversion electron Mössbauer spectroscopy and superconducting quantum interference device magnetometry. The systems show a significant exchange bias effect at low temperatures. Tracer layers of ^{57}Fe (in the Fe layer) and $^{57}FeSn_2$ (in the $FeSn_2$ layer) have been placed in the samples in order to probe the spontaneous spin orientation at different distances from the Fe/$FeSn_2$ interface. The Fe spins in the ferromagnetic layer are preferentially oriented in the interfacial plane. In as-prepared samples the presence of the Fe top layer induces a striking out-of-plane component of the interfacial Fe spins in the antiferromagnetic $FeSn_2$ film. This perpendicular component decreases in magnitude at a larger distance from the interface. A reorientation transition from out-of-plane toward in-plane spin orientation was observed in the interfacial $FeSn_2$ layer with increasing age of the sample. This effect is correlated with an increased magnitude of the exchange bias field for the aged samples.

DOI: 10.1103/PhysRevB.72.064440 PACS number(s): 75.70.Cn, 76.80.+y, 75.30.Gw

I. INTRODUCTION

Exchange bias phenomena are related to the unidirectional anisotropy induced at the interface between a soft ferromagnetic (F) and an antiferromagnetic (AF) material with high magnetic anisotropy, when the system is cooled in an applied magnetic field or in remanence through the Néel temperature (T_N) of the AF phase, while the F phase is magnetically ordered.[1–3] The effect was discovered more than four decades ago.[4] Recent applications, especially in spin-valve type devices[5–10] have renewed the interest in the effect and its underlying physics. Intensive experimental and theoretical work on exchange biased bilayers were performed in the last decade, but the microscopic origin and the role of the different parameters involved in the exchange bias mechanism (magnetic anisotropy, interfacial roughness and spin structure, magnetic domains, etc.) are still a topical subject.[1–3,11–24] Exchange bias phenomena are presently explained by a variety of possible coupling mechanisms.[3,11–24] Common to all microscopic models is the restrictive assumption that the interfacial spin configuration in the AF part is similar to its bulk spin structure. This may not be true due to the reduced coordination and symmetry, roughness, microstructural changes, or lattice mismatch at the F/AF interface. Therefore, the knowledge of the real spin structure at the interface and its relation to the exchange bias field H_E or/and the coercive field H_C is an important issue for the theoretical description and for the prediction of the magnitude of the exchange bias effect in real systems. In this respect, the real orientation of the AF spins relative to the film plane (and implicitly relative to the F spins, which are supposed to show in-plane orientation due to the shape anisotropy) should be important for the various models. In the earlier model of Meiklejohn and Bean[4,12,13] the exchange bias field is proportional to the interaction strength at the F/AF interface, given by the scalar product $\langle S_F \times S_{AF} \rangle = S_F \times S_{AF} \cos\alpha$, with α the angle between the interfacial ferromagnetic (S_F) and antiferromagnetic (S_{AF}) spins. In more advanced models, which assume AF domain formation or random fields, $H_E \sim (K_{AF} A_{AF})^{1/2} \cos\alpha$, with K_{AF} the anisotropy constant and A_{AF} the exchange stiffness of the AF.[1,15] It may be seen that in both cases the magnitude of H_E (experimentally obtained by the shift of the hysteresis loop along the field axis from the symmetrical position) scales with $\cos\alpha$, resulting in symmetrical hysteresis loops (or $H_E = 0$ Oe) for perpendicular orientation between F and AF spins (even when all the other conditions inducing unidirectional anisotropy are fulfilled). The temperature at which H_E becomes zero is called the blocking temperature T_B. For systems with very thin films or small AF grains T_B is often smaller than T_N.[1]

Only a limited number of experimental techniques are able to provide information on the spin structure in buried magnetic interfaces, such as neutron diffraction[25–28] and x-ray magnetic dichroism[29] (also in conjunction with photoemission electron microscopy.[30,31]) Conversion electron Mössbauer spectroscopy (CEMS) is another powerful method, suitable for the atomistic study of the interfacial spin configuration via the nuclear Zeeman effect. Simultaneously, CEMS provides atomistic information about the local structure and symmetry via electric hyperfine (hf) inter-

TABLE I. Nomenclature (label) and sample code of the samples investigated, their geometrical structure, growth temperature T_S of the AF layer, and annealing temperature T_a of the AF layer.

Sample label	Sample code	$FeSn_2$(001)	T_S(°C)	T_a(°C)
AF(int)1	fs5	40 Å Sn/50 Å $^{57}FeSn_2$/350 Å $FeSn_2$/InSb(001)	250	350
AF(int)2	af4	30 Å Sn/50 Å $^{57}FeSn_2$/200 Å $FeSn_2$/InSb(001)	200	350
AF(ctr)	fs7	40 Å Sn/175 Å $FeSn_2$/50 Å $^{57}FeSn_2$/175 Å $FeSn_2$/InSb(001)	250	350
		Fe/$FeSn_2$(001)		
F/AF(int)1	fs4	40 Å Sn/60 Å Fe/50 Å $^{57}FeSn_2$/350 Å $FeSn_2$/InSb(001)	250	350
F/AF(int)2	fs12	40 Å Sn/60 Å Fe/40 Å $^{57}FeSn_2$/240 Å $FeSn_2$/InSb(001)	250	Non-annealed
F(int)/AF(int)	eb3	30 Å Sn/48 Å Fe/12 Å ^{57}Fe/50 Å $^{57}FeSn_2$/200 Å $FeSn_2$/InSb(001)	200	350
F/AF(ctr)	fs6	40 Å Sn/60 Å Fe/175 Å $FeSn_2$/50 Å $^{57}FeSn_2$/175 Å $FeSn_2$/InSb(001)	250	350

actions. The information about the spin orientation and the local magnetic interactions can be obtained with high depth selectivity by using the ^{57}Fe-isotope tracer layer technique, where ^{57}Fe-containing probe layers (enriched in the Mössbauer active isotope ^{57}Fe) are artificially placed at the interface or at different depths in the investigated thin film system.[32–34] Recently, CEMS has been applied to investigate changes in the ferromagnetic spin structure induced by exchange bias in Fe/MnF_2.[35]

In this work we report on the study of the out-of-plane spin component in both, the F and AF part of Fe/$FeSn_2$ bilayer systems. The ^{57}Fe CEMS method in perpendicular geometry (with the gamma radiation perpendicular to the sample plane) was employed in order to fulfil this task. ^{57}Fe enriched tracer layers (12-Å thick ^{57}Fe in the polycrystalline Fe layer and ~50-Å thick $^{57}FeSn_2$ in the $FeSn_2$ epitaxial layer) were used to probe the spin structure at the interfacial region and in certain depths of the magnetic films. A remarkable out-of-plane spin component in the antiferromagnet was found to be induced by the F layer and was correlated with the exchange bias field determined by magnetometry.

II. EXPERIMENT

Antiferromagnetic $FeSn_2$(001) thin films and Fe/$FeSn_2$(001) bilayer systems showing exchange bias effects at low temperatures were obtained by molecular beam epitaxy. The tetragonal $FeSn_2$ phase (a=6.52 Å and c =5.32 Å) has been epitaxially grown in ultrahigh vacuum (UHV) on the clean surface of cubic InSb(001) substrates (a=6.47 Å) by co-evaporation from two sources. Experimental details about the preparation and the structural investigations of the $FeSn_2$ thin films were reported elsewhere.[36,37] The substrate temperature T_S during the growth of the $FeSn_2$ film was between 200 and 250 °C (as required for epitaxy), and was only 50 °C during growth of the polycrystalline Fe overlayer. Thicknesses of 280 and 400 Å were chosen for AF films without Fe coverage, and of 250, 280, and 400 Å in the F/AF bilayer systems. The overall thickness of the Fe film (F) was 60 Å. Tracer layers (50-Å or 40-Å thick $^{57}FeSn_2$ alloy and 12-Å thick ^{57}Fe, respectively), being 95% enriched in the ^{57}Fe Mössbauer isotope and being structurally identical with the base phases, have been grown under identical conditions as for the base phases at different depth from the Fe/$FeSn_2$ interface. (The natural isotopical abundance of ^{57}Fe in the base phases is only 2%.) The systems were covered by 30–40 Å thick Sn cap layers, grown at 50 °C. The geometrical structure of the various samples investigated here, the growth temperature and annealing temperature of the AF layer, and their nomenclature (sample label) are presented in Table I. Before growing the Fe layer, all AF layers (except that of sample F/AF(int)2) were *in situ* annealed at 350 °C in UHV for more than 100 min in order to increase their Néel temperature T_N.[36] The geometrical structure of the samples with the position of the tracer layer/layers are schematically shown in Fig. 1. Néel temperatures higher than 295 K were evidenced by CEMS (see below) in all AF layers, including the non-annealed one. Under optimum annealing conditions, the maximum Néel temperature in such films can approach the T_N value of the bulk $FeSn_2$ phase[36,38] which is about 380 K.[38–41]

The epitaxial growth of the AF $FeSn_2$(001) films was confirmed for every sample by typical *in situ* reflection high-energy electron diffraction (RHEED), and by *ex situ* x-ray diffraction (XRD) patterns.[36,37] The out-of-plane component of the Fe spin structure in both the F and AF phases, was measured at different temperatures in zero external field by ^{57}Fe CEMS in perpendicular geometry (γ-ray direction perpendicular to the sample plane). For CEMS measured down to 80 K, homemade proportional counters (He-CH_4 gas mixture for room temperature (RT) and pure He for lower temperatures) were used. CEM spectra at 10 K were obtained by using a channeltron electron detector placed (together with the sample) in the inner evacuated chamber of a liquid He bath cryostat. A Mössbauer drive system operating in con-

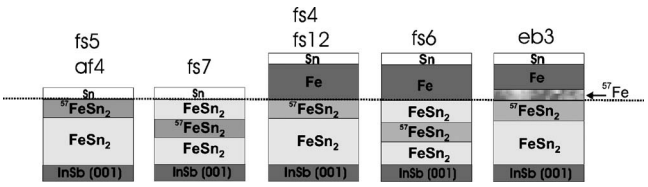

FIG. 1. Schematics of the geometrical structure of the various samples investigated, showing the different positions (depths) of the thin ^{57}Fe and $^{57}FeSn_2$ tracer layers in the Fe layer and/or $FeSn_2$ layer, respectively. The samples are labeled as indicated.

stant acceleration mode combined with conventional electronics and a ^{57}Co source (Rh matrix) of ~50 mCi activity were employed. The source temperature was held constant at room temperature (RT). Due to the chosen geometrical structure of the samples (Table I) more than 90% of the detected conversion electrons following the Mössbauer absorption are generated in the tracer layer/layers enriched in the ^{57}Fe Mössbauer isotope and, therefore, the CEM spectra give depth selective information. The CEM spectra were least-squares fitted by using the computer program NORMOS by Brand.[42] All isomer shift values are given relative to bulk bcc Fe at RT.

The exchange coupling was induced by field-cooling the bilayer systems from 400 K (above T_N) down to the measurement temperature in a magnetic field of 0.05 T applied along the [110] direction of the $FeSn_2(001)$ surface. Temperature dependent hysteresis loops, with the field applied also along the [110] direction, were obtained by superconducting quantum interference device (SQUID) magnetometry. Here, temperature dependent magnetic measurements were performed on sample F/AF(ctr) one week after preparation (as-prepared sample) and again two months after preparation (aged sample). Sample F/AF(ctr) has a similar geometrical structure as sample F/AF(int)1, the only difference being the position of the tracer layer (see Table I).

III. METHODOLOGICAL ASPECTS

Mössbauer spectra obtained in perpendicular geometry (γ-ray perpendicular to the film plane) may provide valuable information about the out-of-plane Fe spin component for each spectroscopically resolved Zeeman-split sextet (each sextet belonging to a certain magnetic phase). The integrated line intensity ratios (spectral area ratios) of the six lines are given by $3:R_{23}:1:1:R_{23}:3$.[43] R_{23} represents the ratio of the (integrated) intensities of the second (or fifth) and the third (or fourth) lines of the Mössbauer sextet, given by $R_{23}(\theta) = 4\sin^2\theta/(1+\cos^2\theta)$, with θ the angle between the Fe spin direction and the γ-ray direction. From measured R_{23} values one obtains the model independent parameter $\langle\cos^2\theta\rangle$, where the brackets indicate averaging over the angular spin distribution in the sample. For the extreme case of complete out-of-plane spin orientation ($\theta=0°$)$R_{23}=0$, while for complete in-plane orientation ($\theta=90°$)$R_{23}=4$. Due to possible superpositions of different subspectra in the central part of the measured Mössbauer spectrum, changes in the intensity ratio R_{23} may be easier detected more often by observing the intensity ratio of the second (fifth) line and the first (sixth) line of the sextets. In perpendicular geometry, the above relation can be used also in the form $R_{23}(\alpha)=4\cos^2\alpha/(2-\cos^2\alpha)$, where $\alpha=90°-\theta$ is the angle between the Fe spin direction and the sample plane. In order to determine the spin structure, the general algorithm[44–46] for different angular Fe spin distributions (spin texture) was applied to the case of the perpendicular CEMS geometry in the present work. Accordingly, for a theoretical angular out-of-plane spin distribution $P(\alpha)$, the experimental intensity ratio R_{23} is given by

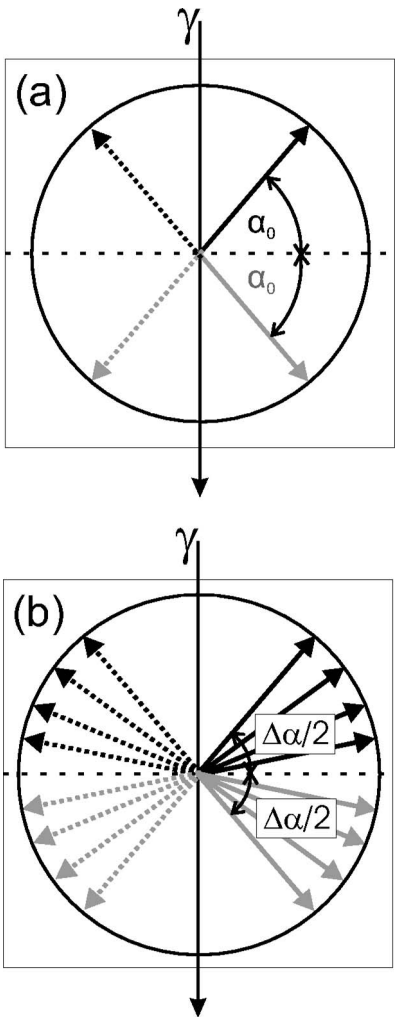

FIG. 2. Schematic representation of the angular distribution of the out-of-plane Fe spin component in an arbitrary plane perpendicular to the film surface for two models: unidirectional (a) and step shaped spin-fanning structure (b). The angular spin distributions show cylindrical symmetry relative to the film normal (or γ-ray direction).

$$R_{23} = 4\frac{\langle\cos^2\alpha\rangle}{2-\langle\cos^2\alpha\rangle} \text{ with}$$

$$\langle\cos^2\alpha\rangle = \int_{-\pi}^{+\pi} P(\alpha)\cos^2\alpha\, d\alpha \quad \text{and}$$

$$\int_{-\pi}^{+\pi} P(\alpha)d\alpha = 1. \tag{1}$$

R_{23} may be calculated from Eq. (1) for a particular model spin distribution $P(\alpha)$ and compared with the experimental R_{23} value.

In the simplest model, the unidirectional model, all Fe spins are assumed to point to only one direction relative to the sample plane [Fig. 2(a)]. This corresponds to a Dirac-type probability distribution $P(\alpha)=\delta(\alpha-\alpha_0)$. Then Eq. (1) becomes

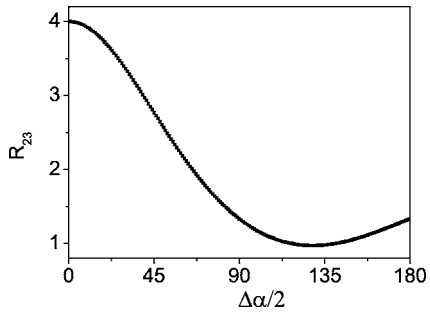

FIG. 3. Theoretical line intensity ratio R_{23} versus the semiaperture $\Delta\alpha/2$ for an out-of-plane step-shaped angular Fe spin distribution (spin-fanning model).

$$R_{23} = 4\cos^2\alpha_0/(2-\cos^2\alpha_0) \tag{2}$$

and cos α_0 or, alternatively, the Fe spin orientation α_0, can be directly derived from a measurement of R_{23}. For a more realistic spin structure (e.g., near a rough interface containing defects), the step-shaped angular distribution describing an out-of-plane spin-fanning structure [Fig. 2(b)] may be useful. In this situation the spins are oriented with equal probability only within an angular aperture $\Delta\alpha$. (This angular distribution is centered along a direction in the sample plane.) Then, the probability is expressed as $P(\alpha)=1/\Delta\alpha$ for $-\Delta\alpha/2<\alpha<\Delta\alpha/2$, and $P(\alpha)=0$ in the rest of the 2π interval, and Eq. (1) becomes

$$R_{23} = 4\frac{1+(\sin\Delta\alpha)/\Delta\alpha}{3-(\sin\Delta\alpha)/\Delta\alpha}, \quad \text{since}$$

$$\langle\cos^2\alpha\rangle = \frac{[1+(\sin\Delta\alpha)/\Delta\alpha]}{2}. \tag{3}$$

The dependence of the R_{23} ratio on the out-of-plane angular spin semiaperture $\Delta\alpha/2$, as obtained by numerical integration of Eq. (3), is presented in Fig. 3. The angular semiaperture $\Delta\alpha/2$ is determined from this theoretical curve and from the experimental R_{23} ratio. We emphasize that this model works properly only for intensity ratios $R_{23}>0.97$ (or $\Delta\alpha/2<129°$. Values $R_{23}<1.3$ can be interpreted only in the frame of a fanning spin structure centered along the direction perpendicular to the sample plane.

IV. RESULTS AND DISCUSSION

A. Spin structure in antiferromagnetic $FeSn_2$ single layers

According to the AF spin structure in bulk $FeSn_2$,[38–41] the Fe spins are arranged within the (001) planes of tetragonal $FeSn_2$, i.e., perpendicular to the c axis. Therefore, the Fe spins are expected to be oriented in the plane of our $FeSn_2$(001) films.

The RT CEM spectra of the AF samples AF(int)1 [interfacial $^{57}FeSn_2$ tracer layer) and AF(ctr) (central $^{57}FeSn_2$ tracer layer) are shown in Fig. 4. Also displayed in Fig. 4 are CEM spectra of sample AF(int)2 [interfacial $^{57}FeSn_2$ tracer layer, but with a 50 °C lower growth temperature and a thinner overall AF layer, as compared to samples AF(int)1 and AF(ctr)] measured at RT and 50 K, respectively. The 50-K spectrum could be satisfactorily fitted with one magnetic component (sextet-S3) presenting a hyperfine magnetic field B_{hf} of 15.5(1) T and an isomer shift of 0.640(3) mm/s. Both spectral parameters are typical for the AF ordered $FeSn_2$ phase.[36–41] For sample AF(int)2 at RT, the magnetically ordered phase gives rise to a sextet (sextet S3) with $B_{hf}=10$ T and an isomer shift of 0.501(2) mm/s. The difference in isomer shifts at RT and 50 K is caused by the second-order Doppler (SOD) shift (relativistic center shift of the spectra with T). The fitting of the RT spectra of sample AF(int)2 and of all the other epitaxial $FeSn_2$ thin-film samples required the consideration of an additional broad central pattern P (singlet or doublet, depending on the preparation conditions) with an isomer shift of about 0.55 mm/s. Taking into account the very similar isomer shifts at RT of the two patterns S3 and P as well as the fact that pattern P disappears at 50 K, both

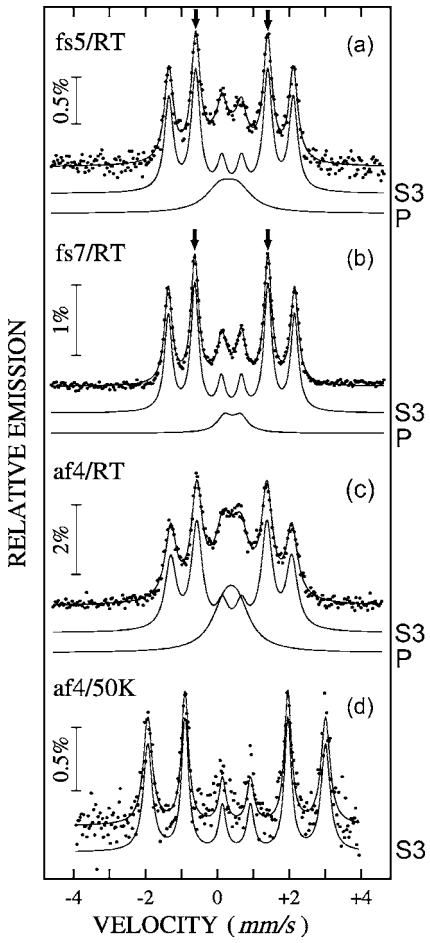

FIG. 4. CEM spectra of samples AF(int)1, AF(ctr), and AF(int)2 [consisting only in the antiferromagnetic $FeSn_2$(001) layer] obtained in perpendicular geometry (γ-ray perpendicular to the sample plane). Samples AF(int)1 (interfacial $^{57}FeSn_2$ tracer layer) (a) and AF(ctr) (centered $^{57}FeSn_2$ tracer layer) (b) were studied at RT, whereas sample AF(int)2 (interfacial $^{57}FeSn_2$ tracer layer, but slightly different preparation conditions) was investigated both, at RT (c) and at 50 K (d). The spectra were least-squares fitted with a broad central paramagnetic feature P (singlet or doublet) and/or the sextet S3 of AF $FeSn_2$.

components (S3 and *P*) in the RT CEM spectra have to correspond to different magnetic environments of the same tetragonal $FeSn_2$ phase. This situation has been interpreted in the following terms:[36,37] The presence of defects in the $FeSn_2$ layer (presumably antisite occupation of Fe and Sn atoms and/or deviations from stoichiometry) will weaken the long-range magnetic interactions between the Fe atomic magnetic moments. A certain spatial inhomogeneity of the defect-associated $FeSn_2$ regions leads to a fluctuating density of defects throughout the AF sample volume. In the "high defect" volumes of the AF phase, the long-range magnetic interactions may be reduced even down to zero at temperatures lower than the Néel temperature of the ordered (stoichiometric) $FeSn_2$ phase. Such Fe atoms in defect regions will experience lower molecular fields and, consequently, lower hyperfine magnetic fields B_{hf}, thus contributing to the broad central spectral component *P* at RT. Following this picture, Fe atoms carrying a continuous distribution of time-averaged magnetic moments and, hence, hyperfine magnetic fields, are spread out over the AF sample volume. Therefore, the most suitable fit of the RT CEM spectra should be done with a continuous distribution of B_{hf}, starting from 0 T. In this model, lower hyperfine fields would correspond to regions with a higher density of defects and vice versa. We have chosen the fitting solution with two distinct Mössbauer components (one magnetic S3 and one paramagnetic *P*) because: (i) the distribution of B_{hf} obtained by the alternative fitting procedure shows mainly two local maxima centered at about 10 T and close to 0 T, respectively; (ii) it offers the advantage of a more precise determination of the R_{23} ratio of the magnetic sextet (S3), and (iii) the relative areas of the two spectral components (S3 and *P*) provide a measure of the degree of disorder in the antiferromagnetic phase. [E.g., a higher relative spectral area of the paramagnetic component (*P*) indicates a higher degree of atomic disorder.] It is clear that, based on the above considerations, the broad central component *P* ("defect line") takes into account both a pure paramagnetic line and a nearly collapsed magnetic pattern due to thermally rapidly fluctuating magnetic regions in the chemically disordered volumes of $FeSn_2$. The magnetic moments of the iron atoms in the "defect" volumes may freeze at lower temperatures, e.g., in a spin glasslike state, thus increasing gradually the relative contribution of the magnetic sextet S3 in the low temperature CEM spectra upon cooling. Moreover, the central Fe atom will experience different electric field gradients down to zero, depending on the number of defects, e.g., antisite atoms in its local neighborhood. Accordingly, the central component in the CEM spectrum may also include a distribution of electric quadrupole splittings, whose characteristics are sensitive to the specific preparation conditions. Such distributions centered at a finite (mean) quadrupole splitting are presented in the RT CEM spectra of samples AF(int)1 and AF(ctr) by the broad central doublet *P*, whereas a distribution centered at zero quadrupole splitting is represented by the broad central singlet *P* in the RT spectrum of sample AF(int)2 (Fig. 4).

Values of the measured intensity ratio R_{23} and of $\langle \cos^2 \alpha \rangle$ for the AF ordered $FeSn_2$ phase are given in Table II for all the samples studied here. Also presented in Table II are the parameters α_0 and $\Delta\alpha/2$ of the angular spin distributions computed from the measured R_{23} values for the unidirectional model and perpendicular fanning model, respectively.

As can be observed in Fig. 4 and Table II, the Fe spins are oriented completely in the sample plane at RT ($R_{23}=4$ within error bars) at both the $Sn/FeSn_2$ interface [samples AF(int)1 and AF(int)2] and in the center [sample AF(ctr)] of the AF $FeSn_2(001)$ thin film. This is expected considering the spin structure of the bulk $FeSn_2$.[38–41] Our result proves that (at room temperature) the Sn cap layer, if in direct contact with the $FeSn_2$ layer, has no effect on its spin structure. The degree of disorder is higher in sample AF(int)2 (higher relative spectral area of the paramagnetic feature *P*) as compared to samples AF(int)1 and AF(ctr), mainly due to the lower film growth temperature for AF(int)2 (Table I).[36] It is interesting that a stronger paramagnetic component is observed in sample AF(int)1 with its tracer layer at the film interface as compared to sample AF(ctr) with its tracer layer in the center of the film. The higher chemical disorder in sample AF(int)1 with its interfacial tracer layer may be due to additional defects induced by atomic interdiffusion at the interface with the Sn cap layer.

After cooling sample AF(int)2 to 50 K, an out-of-plane component of the Fe spins located at the interface of the antiferromagnetic $FeSn_2$ films is induced (with $\Delta\alpha/2=43°$ for the spin fanning structure). This is surprising, because according to the known spin structure of bulk AF $FeSn_2$ (Refs. 39–41) the Fe spins are expected to lie within the (001) planes perpendicular to the *c* axis, i.e., in the plane of our epitaxial $FeSn_2(001)$ films. The evolution of the out-of-plane spin component upon cooling could be caused by magnetoelastic effects and mechanical stress in the film due to different thermal expansion coefficients between film and substrate. At 200 K, for instance, the thermal expansion coefficient α of InSb (substrate) is 4.67×10^{-6} K^{-1}, while α of Sn (cap layer) is 20.7×10^{-6} K^{-1} (obtained by averaging along and perpendicular to the *c* axis of the tetragonal Sn).[47] Since α of $FeSn_2$ is unknown to our knowledge, we can only estimate this value by interpolating between α of bcc Fe (9.96×10^{-6} K^{-1}) and Sn, considering the composition of $FeSn_2$. This yields $\alpha\approx17\times10^{-6}$ K^{-1} for $FeSn_2$, which is much larger than α of InSb, but comparable to α of Sn. We may conclude that the stress exerted on the $FeSn_2$ film upon cooling is probably dominated by the effect of the InSb substrate, while the influence of the Sn cap layer is very likely much smaller.

B. Influence of the Fe top layer

The RT CEM spectra of the bilayer samples F/AF(int)1 (interfacial $^{57}FeSn_2$ tracer layer) and F/AF(ctr) ($^{57}FeSn_2$ tracer layer in the center of the AF film) are shown in Fig. 5. We like to emphasize that sample F/AF(int)1 [F/AF(ctr)] is identical to sample AF(int)1 [AF(ctr)] in the geometrical structure of their AF phase, the only difference being the addition of the ferromagnetic Fe layer on the top of the $FeSn_2$ films. Therefore, an additional weak magnetic pattern (S2) appears in the CEM spectra of the bilayer systems, originating from the natural bcc-Fe top layer (which has a ^{57}Fe natural abundance of only 2%).

TABLE II. Measured line intensity ratio R_{23} and $\langle\cos^2\alpha\rangle$ values for the magnetic spectral components belonging to both the F and AF tracer layers, as obtained from CEM spectra taken at different temperatures and in different preparation states of the samples. Also given are the angles α_0 and $\Delta\alpha/2$ of the out-of-plane angular spin distributions computed for the two models (unidirectional and spin-fanning structure, respectively). (as-prepared=maximum of one week after sample preparation, aged=two months after preparation).

Sample label	Measurement Temperature (K)	Field-cooling	Preparation stage	Magnetic phases	R_{23}	$\langle\cos^2\alpha\rangle$	α_0(degrees)	$\Delta\alpha/2$(degrees)
AF(int)1	295	No	As-prepared	AF	3.9(1)	0.997	4(3)	10(5)
AF(ctr)	295			AF	4.0(1)	1	0(3)	0(5)
AF(int)2	295			AF	4.0(2)	1	0(5)	0(10)
	50			AF	2.9(2)	0.841	24(3)	42(5)
F/AF(int)1	295	No	As-prepared	AF	1.5(1)	0.545	43(3)	84(3)
		Yes		AF	1.3(1)	0.490	46(3)	93(3)
			Aged	AF	3.7(1)	0.961	11(3)	20(3)
F/AF(ctr)	295	No	As-prepared	AF	2.5(1)	0.771	29(3)	52(3)
F(int)/AF(int)	295	No	As-prepared	FM	3.9(2)	0.997	4(5)	10(10)
				AF	2.9(2)	0.841	24(5)	42(5)
		Yes		FM	4.0(2)	1	0(5)	0(10)
				AF	2.5(2)	0.771	29(5)	52(5)
	10	No		FM	3.7(2)	0.961	11(5)	20(5)
				AF	2.0(1)	0.667	35(3)	65(3)
		Yes		FM	3.7(2)	0.961	11(5)	20(5)
				AF	2.0(1)	0.667	35(3)	65(3)
F/AF(int)2	295	Yes	As-prepared	AF	2.4(1)	0.75	30(3)	55(3)
			Aged	AF	3.8(1)	0.974	9(3)	17(4)
	220			AF	3.0(1)	0.857	22(3)	39(3)
	150			AF	2.7(1)	0.806	26(3)	47(3)
	80			AF	2.7(1)	0.806	26(3)	47(3)

By comparing Figs. 4(a) and 5(a), or Figs. 4(b) and 5(b), a drastic change in the intensity ratio R_{23} of the Mössbauer sextet S3 belonging to the AF $FeSn_2$ phase can be observed (see arrows in the two figures), which is induced by the presence of the Fe top layer. Accordingly, sample F/AF(int)1 with its bilayer structure and interfacial $^{57}FeSn_2$ tracer layer shows a mean orientation of the interfacial Fe spins in the AF phase of $\Delta\alpha/2=100°$ (for the spin fanning structure). These values should be compared with $\Delta\alpha/2\approx5°$ for the $FeSn_2$ layer in sample AF(int)1, indicating nearly in-plane orientation of the Fe spins in sample AF(int)1. The Fe spins in the $^{57}FeSn_2$ tracer layer placed at the center of the AF film rotate from the in-plane position in sample AF(ctr) (AF single layer) up to a value of $\Delta\alpha/2=55°$ (in the fanning model) in sample F/AF(ctr) (F/AF bilayer system). This demonstrates that the out-of-plane component of the Fe spins in the AF phase, induced by the presence of the F top layer, is much stronger at the F/AF interface than in the center of the AF phase. The strong out-of-plane spin component in the AF layers was observed in all the $Fe/FeSn_2$ systems investigated within a short time after preparation, the magnitude of the effect being controlled to some degree by the preparation conditions.

We assume that the driving force for the spin rotation in the AF is of magnetoelastic origin via spin orbit interaction, and presumably is due to the stress exerted by the Fe top layer on the AF $FeSn_2$ layer. It is unlikely that the Sn cap layer is responsible for the stress on the $FeSn_2$ layer, since there is a spacer layer of Fe between the Sn cap layer and the $FeSn_2$ layer, and since Sn is a mechanically soft material that can be easily plastically deformed by introducing dislocations. Therefore, mechanical stress in the soft Sn cap layer will easily be relieved by formation of misfit dislocations, contrary to the mechanically harder materials Fe and $FeSn_2$.

C. Effect of the cooling field

An even stronger out-of-plane Fe-spin component in the AF interfacial layer is evidenced in the RT CEM spectra after field cooling the bilayer system below the Néel temperature of the AF phase in a magnetic field of 0.05 T. CEM spectra of sample F(int)/AF(int), taken at RT and 10 K, before and after the field cooling procedure, respectively, are presented in Fig. 6. [$T_N\approx380$ K for sample F(int)/AF(int), see Ref. 37]. The more complex spectra of this sample are due to the fact that the bilayer system F(int)/AF(int) contains two interfacial tracer layers, placed on either side of the $Fe/FeSn_2$ interface (one on the F side and another on the AF side, see Table I and Fig. 1). Accordingly, the CEM spectra were fitted with three magnetic components and a paramagnetic one. The two outer sextets (*S*1 and *S*2) with hyperfine magnetic fields of about 31 and 33 T, respectively, and almost negligible isomer shifts at RT, were assigned to a Sn-impurity containing interfacial bcc-Fe layer and a nearly pure bulklike

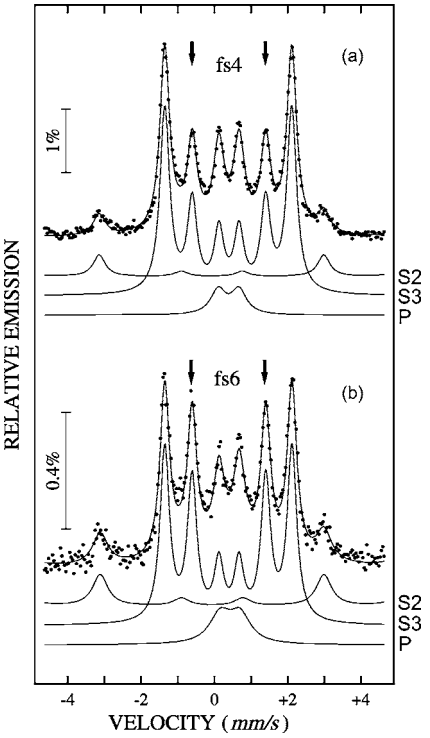

FIG. 5. CEM spectra of sample F/AF(int)1 (with $^{57}FeSn_2$ tracer layer at the $Fe/FeSn_2$ interface)(a) and F/AF(ctr) (with $^{57}FeSn_2$ tracer layer in the center of the $FeSn_2$ film)(b), obtained at RT in perpendicular geometry. Sample F/AF(int)1 [F/AF(ctr)] differs from sample AF(int)1 [AF(ctr)] only by the presence of the Fe top layer. A significant change of the intensity ratio R_{23} (see arrows) can be observed, as compared to the single layer $FeSn_2$ systems [AF(int)1 and AF(ctr)] presented in Fig. 4. (The natural Fe top layer produces the spectral component S2, in this case the inner four lines of the bcc-Fe sextet *S*2.)

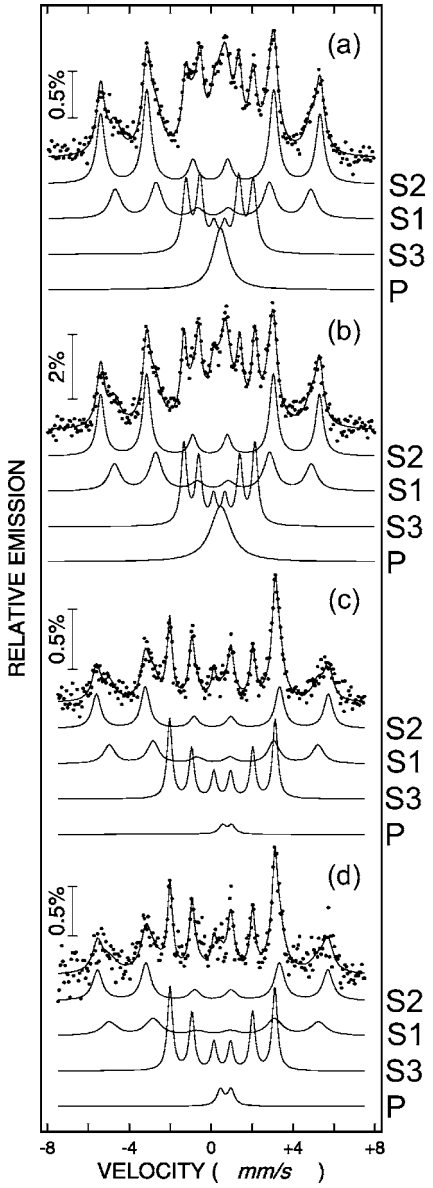

FIG. 6. CEM spectra of sample F(int)/AF(int) (tracer layers on either site of the $Fe/FeSn_2$ interface) measured at RT (a),(b) and 10 K (c),(d) and in perpendicular geometry. The CEMS measurements were performed before and after field cooling [field-cooled cases correspond to (b) and (d)]. The fitted subspectra originate from an interfacial bcc-Fe layer containing interdiffused Sn impurities (S1), a pure bulklike bcc-Fe layer farther away from the F/AF interface (S2), an AF $FeSn_2$ layer (S3), and a paramagnetic central feature (broad singlet or weak doublet) due to defect regions in the AF.

bcc-Fe layer [isomer shift of 0.057(7) mm/s] farther away from the $Fe/FeSn_2$ interface, respectively.[37] Due to the overlapping lines of sextets S1 and *S*2, the same R_{23} ratio was assumed for *S*1 and *S*2 in the least-squares fitting. As mentioned above, the inner sextet *S*3, with an isomer shift of 0.504(7) mm/s and a much smaller hyperfine magnetic field ($B_{hf} \approx 10$ T) at RT, was again assigned to the chemically ordered stoichiometric $FeSn_2$ phase presenting long-range AF ordering at RT. The paramagnetic central component *P* (singlet or doublet) originates from chemically disordered regions in the $FeSn_2$ phase. By decreasing the temperature, the Fe magnetic moments of the disordered phase gradually become frozen in the AF matrix, leading to a gradually increasing spectral contribution of the inner sextet S3 at the expense of the central paramagnetic pattern *P*.

At RT, the interfacial Fe spins in the F layer are completely aligned in the film plane ($R_{23}=4.0$), both before and after field cooling the bilayer system through T_N [Table II, sample F(int)/AF(int)]. To the contrary, the interfacial Fe spins in the AF $FeSn_2$ layer, presenting already an initial out-of-plane component ($\Delta\alpha/2=43°$), will further rotate out of the film plane (up to $\Delta\alpha/2=55°$) after the field cooling procedure. In spite of the relatively small increment of the out-of-plane spin component induced by field cooling, the effect was regularly observed at RT on all magnetic bilayers [e.g., for sample F/AF(int)1, $\Delta\alpha/2=100°$ in the initial state, as compared to $\Delta\alpha/2=120°$ after field cooling, Table II]. However, field cooling does not affect the out-of-plane spin component in the AF layer at 10 K, where exchange bias effects are observed (see Ref. 37, and Secs. IV E and IV F). In spite of a stronger out-of-plane component of the Fe spins in the interfacial AF layer of sample F(int)AF(int) at 10 K (with $\Delta\alpha/2=73°$) as compared to the RT case, this out-of-

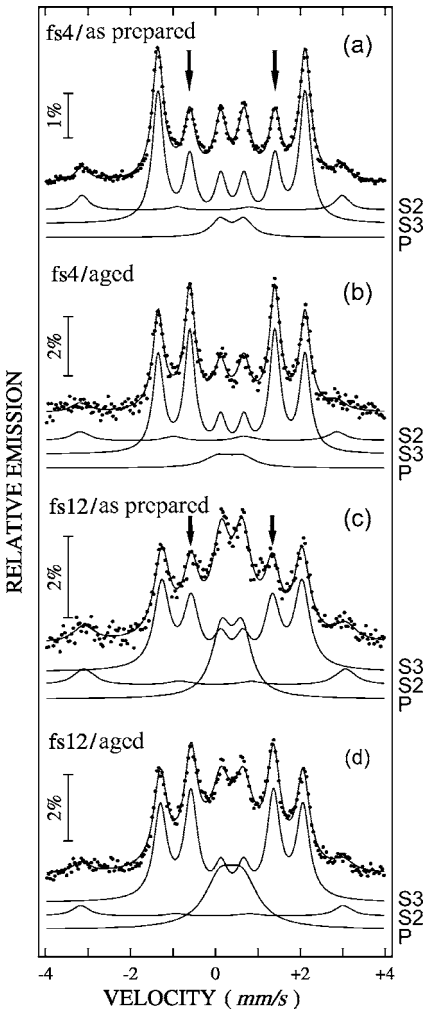

FIG. 7. CEM spectra of samples F/AF(int)1 (a),(b) and F/AF(int)2 (c),(d) at RT in perpendicular geometry. "As-prepared" [(a),(c)] refers to a measurement performed within less than one week after sample preparation, and "aged" refers to a measurement performed two months later. The samples were stored at RT. The significant change of the intensity ratio R_{23} upon aging is indicated by the arrows.

plane spin component is similar for the initial (zero-field cooled) state at 10 K and after field cooling to 10 K ($\Delta\alpha/2=73°$, Table II). At 10 K the interfacial Fe spins in the F layer show also a small out-of-plane component [$\Delta\alpha/2=19°$ for F(int)/AF(int)], probably due to the stronger coupling to the canted interfacial Fe spins of the AF phase.

Due to the SOD shift the center shift increases slightly upon cooling to 10 K, namely, from 0.057(7) mm/s at RT to 0.06(2) mm/s at 10 K for the bulklike bcc-Fe layer, and from 0.504(7) mm/s at RT to 0.543(7) mm/s at 10 K for the $FeSn_2$ layer.

D. Time dependent relaxation effects

Figure 7 shows CEM spectra of samples F/AF(int)1 ($Fe/FeSn_2$ bilayer with interfacial $^{57}FeSn_2$ tracer layer and with an annealed AF $FeSn_2$ layer of 400 Å total thickness) and F/AF(int)2 ($Fe/FeSn_2$ bilayer with interfacial $^{57}FeSn_2$ tracer layer and with a nonannealed AF $FeSn_2$ layer of 280 Å total thickness). These systems were measured at RT after the field-cooling procedure and at different time intervals after the preparation: (i) within less than one week (as-prepared sample) and (ii) after two months (aged sample). A significant increase of the intensity ratio R_{23} of sextet $S3$ (belonging to the $FeSn_2$ interfacial phase) is observed for the aged samples as compared to the as-prepared samples (see also Table II), suggesting time dependent reorientation processes of the AF spins toward the in-plane direction. The decrease of the out-of-plane components depends to some extent on the preparation conditions, and for the present case the spin fanning angle $\Delta\alpha/2$ was reduced after two months from $\Delta\alpha/2=120°$ to $\Delta\alpha/2=19°$ in sample F/AF(int)1, and from $\Delta\alpha/2=60°$ to $\Delta\alpha/2=14°$ in sample F/AF(int)2 (Table II). This effect is most likely due to a time dependent structural relaxation at the F/AF interface relieving the stress exerted by the Fe top layer on the AF $FeSn_2$ layer. According to our present observations, the usual thermal annealing treatment of the as-prepared $Fe/FeSn_2$ bilayer cannot remove the interfacial stress (and cannot remove the out-of-plane spin component in the AF), maybe due to additional temperature activated interdiffusion processes that prevent stress relief.

E. Temperature dependent out-of-plane spin component in $Fe/FeSn_2$

Temperature dependent CEM spectra were measured on sample F/AF(int)2 two months after preparation, and after the field-cooling procedure (Fig. 8). Besides the decreasing spectral contribution of the central paramagnetic "defect" feature P already discussed in the previous sections, a clear decrease of the intensity ratio R_{23} of the sextet $S3$ belonging to the interfacial AF $FeSn_2$ phase is observed upon cooling and, consequently, an increase of the out-of-plane spin component in the AF phase at low temperatures. The parameters describing the spin structure in the considered models ($\langle\cos^2\alpha\rangle$, α_0 and $\Delta\alpha/2$) are presented in Table II. The center shift increases upon cooling due to the SOD shift. For the $FeSn_2$ layer we find center-shift values of 0.495(1) mm/s at RT, 0.546(4) mm/s at 220 K, 0.594(1) mm/s at 150 K, and 0.624(2) mm/s at 80 K. The corresponding values for the bulk-like Fe layer are −0.04(5) mm/s, 0.08(7) mm/s, 0.1(1) mm/s, and 0.0(8) mm/s, respectively.

The temperature evolution of the intensity ratio R_{23} of the interfacial AF phase for the aged sample F/AF(int)2 and for the as-prepared sample F(int)/AF(int) are shown in Fig. 9. In the same figure also the R_{23} values of sample F/AF(int)2 (as-prepared) and F/AF(int)1 (as-prepared and aged) are plotted. It is assumed in the following that the R_{23} ratio of the AF phase in as-prepared bilayer samples shows a similar temperature dependence as in the as-prepared sample F(int)/AF(int), whereas the temperature dependence of the R_{23} ratio of the AF phase in the aged samples is assumed to be similar to that in the aged bilayer sample F/AF(int)2. Accordingly, R_{23} values of about 2.5 at 5 K can be derived for both aged bilayers F/AF(int)2 and F/AF(int)1, which have very similar R_{23} ratios at RT (Fig. 9). Further, an R_{23} value of about 0.7 at 5 K may be deduced for the as-prepared bilayer sample

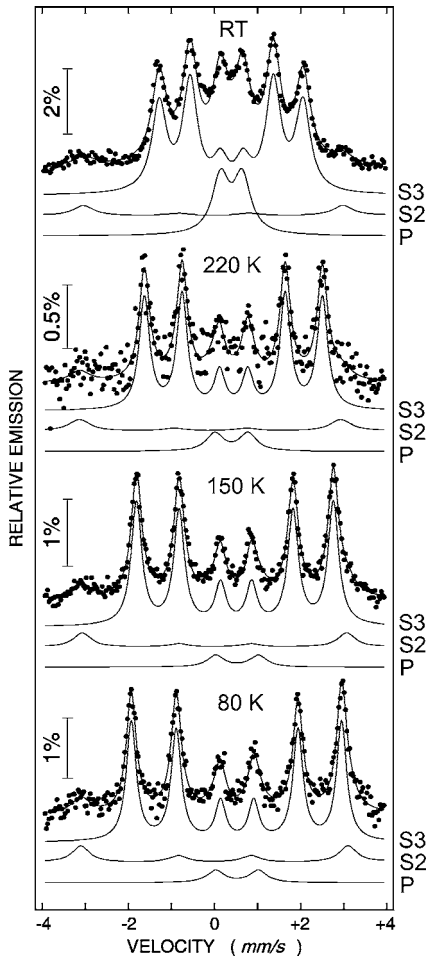

FIG. 8. CEM spectra of the aged sample F/AF(int)2 measured in perpendicular geometry at RT, 220, 150, and 80 K (from top to bottom, respectively).

F/AF(int)1. These R_{23} ratios correspond to the following values of $\cos\alpha_0$ at 5 K in the unidirectional model: $\cos\alpha_0 \sim 0.88$ for the aged samples F/AF(int)2 and F/AF(int)1, and $\cos\alpha_0 \sim 0.54$ for the as-prepared sample F/AF(int)1. It should be noted that in this case α_0 is the average angle between the interfacial AF spins and the interfacial Fe spin direction in the ferromagnetic Fe overlayer, the latter being in-plane oriented (Table II).

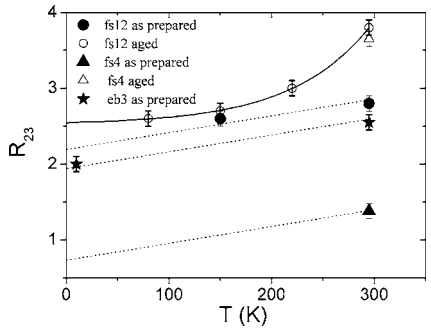

FIG. 9. Intensity ratio R_{23} for the interfacial AF $^{57}FeSn_2$ layer obtained on different samples [F(int)/AF(int), F/AF(int)1, and F/AF(int)2, respectively] and at different temperatures. The full symbols refer to as-prepared samples and the open ones to the aged samples.

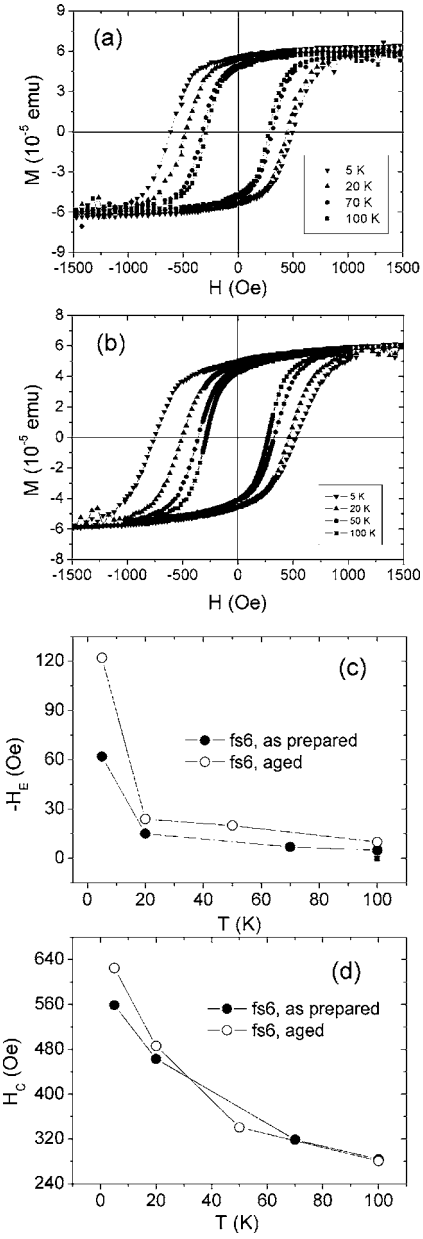

FIG. 10. Hysteresis loops measured by SQUID at different temperatures on sample F/AF(ctr) in the as-prepared state (a) and in the aged state (b). The loops were recorded under the same conditions. Temperature dependence of the exchange field $-H_E$ (c) and the coercive field H_C (d) for the as prepared (full circles) and aged (open circles) sample F/AF(ctr). [F/AF(ctr) has similar geometrical structure and was prepared under similar conditions as sample F/AF(int)1.]

F. Correlation between exchange bias field and out-of-plane spin component in the AF layer

The hysteresis loops obtained at different temperatures on the as-prepared sample F/AF(ctr) (after field cooling in 0.05 T from above T_N down to the measurement temperature) are

shown in Fig. 10(a). Figure 10(b) exhibits hysteresis loops measured under similar conditions on the aged sample F/AF(ctr). The temperature dependences of H_E and H_C are shown in Figs. 10(c) and 10(d), respectively. Starting at 5 K, $|H_E|$ is sharply reduced with increasing temperature in a first step (up to 20 K), and then decreases smoothly down to zero at a blocking temperature T_B of about 100 K. T_B is much lower than T_N, which is above RT. It is evident that below 20 K higher values of $|H_E|$ exist for the aged sample than for the as-prepared sample. For instance, at 5 K $|H_E|$ increases after two months from 64 Oe in the as-prepared sample F/AF(ctr) up to 122 Oe in the aged sample F/AF(ctr). Quantitatively, at 5 K $|H_E|$ is $\sim$1.9 times larger in the aged sample than in the as-prepared sample F/AF(ctr) [Fig. 10(c)]. H_C at low temperature is also higher in the aged sample than in the as-prepared sample [Fig. 10(d)], but the relative change is smaller than that for $|H_E|$.

Due to their similar geometrical structure and preparation conditions (the only difference being the position of the $^{57}FeSn_2$ tracer layer), samples F/AF(ctr) and F/AF(int)1 should behave similarly in their macroscopic magnetic properties, including H_E. As described in Sec. IV E, the mean relative orientation between the interfacial Fe spins in the AF film and the interfacial Fe spins in the F film is taken into account by $\cos \alpha_0$, which is 0.54 in the as-prepared sample F/AF(int)1, and 0.88 in the aged sample F/AF(int)/1, i.e., it is 1.6 times larger in the aged sample. This should be compared with the factor of 1.9 between $|H_E|$ of the aged and as-prepared sample F/AF(ctr). Obviously, there is evidence for a qualitative correlation between $|H_E|$ and $\cos \alpha_0$. It is difficult to say at this stage, if the larger factor of 1.9 for the exchange bias fields as compared to the factor of 1.6 for the corresponding $\cos \alpha_0$ values is due to inherent experimental uncertainties and inaccurate assumptions (e.g., the extrapolation of the out-of-plane spin component at 5 K, Fig. 9), or from a deviation of the linear scaling law $H_E \sim \cos \alpha_0$. However, our result supports a direct anticorrelation between the magnitude of H_E and the out-of-plane interfacial spin component in the AF layer. Moreover, we may suppose that the main reason for the increase in magnitude of H_E with the aging time of the sample is related to the aging-time dependence of the out-of-plane component of the interfacial AF $FeSn_2$ spins, which is very likely finally connected with the relaxation of interfacial stress. Hence, generally magnetoelastic effects in the antiferromagnet could play an important role in the behavior of exchange biased systems.

V. CONCLUSIONS

Antiferromagnetic (AF) epitaxial $FeSn_2(001)$ thin films and exchange coupled $Fe/FeSn_2(001)$ magnetic bilayers were grown by molecular beam epitaxy (MBE) on clean InSb(001) substrates. Tracer layers of $^{57}FeSn_2$ (in the $FeSn_2$ layer) and ^{57}Fe (in the Fe layer) with similar crystallographic structure as the base phases were placed at and away from the F/AF interface in order to study the out-of-plane spin components of the constituent layers by ^{57}Fe CEMS. The measurement of the Mössbauer line intensity ratio R_{23} provided a model-independent way to determine $\langle \cos^2 \alpha \rangle$, with α being the angle between the film normal direction and the Fe spin direction. Models of the mean unidirectional spin orientation and of the step-shaped angular spin distribution were used for a quantitative characterization of the Fe spin structure.

The Fe spins in the AF $FeSn_2$ single-layer films show a nearly complete in-plane orientation at RT and a weak out-of-plane component at low temperatures. A remarkable increase of the out-of-plane spin component of the interfacial AF spins is obtained by growing an Fe layer over the $FeSn_2$ layer. The out-of-plane spin component decreases with the distance from the F/AF interface. It is assumed that this behavior is related to magnetoelastic effects due to stress caused by the lattice mismatch of Fe and $FeSn_2(001)$. Field-cooling procedures induce an additional small increase in the out-of-plane spin component at RT, while this effect is found to be almost negligible at low temperatures, where a strong exchange bias effect is present.

The interfacial Fe spins in the ferromagnetic (F) layer are almost completely aligned in the plane of the F/AF interface at RT, whereas a very weak out-of-plane component was observed at 10 K, probably due to the stronger exchange coupling with the canted interfacial Fe spins of the AF phase.

A drastic reorientation from preferred out-of-plane toward in-plane spin direction in the AF has been observed after keeping the as-prepared $Fe/FeSn_2$ samples at RT for two months (aged samples). This effect may be caused by time dependent stress relief via lattice relaxation at the interface at RT. The behavior of the out-of-plane spin component at different measurement temperatures was analyzed in both, as-prepared and aged samples.

Larger exchange bias fields were observed by SQUID magnetometry for the aged sample than for to the as-prepared state. This increase in magnitude of H_E is explained by the spin reorientation from out-of-plane to in-plane. Further experiments are in progress in such relaxing exchange bias systems in order to determine the exact scaling law between H_E and the mean angle between the interfacial Fe and interfacial AF spins. Generally, magnetoelastic effects in the antiferromagnet could play an important role in the behavior of exchange-biased F/AF bilayers, in particular in systems containing heavy atoms with large spin orbit coupling.

ACKNOWLEDGMENTS

We are grateful to U. v. Hörsten for his expertise technical assistance. V. E. K. appreciates the financial support by the Alexander-von-Humboldt Stiftung and by the Romanian Program No. CERES 3-89/2003. Financial support by the Deutsche Forschungsgemeinschaft (SFB 491) is gratefully acknowledged.

*Corresponding author. Electronic address: keune@uni-duisburg.de

[1] J. Nogués and I. K. Schuller, J. Magn. Magn. Mater. **192**, 203 (1999).
[2] A. E. Berkowitz and K. Takano, J. Magn. Magn. Mater. **200**, 552 (1999).
[3] R. L. Stamps, J. Phys. D **33**, R247 (2000).
[4] W. H. Meiklejohn and C. P. Bean, Phys. Rev. **102**, 1413 (1956).
[5] B. Dieny, V. S. Speriosu, S. S. P. Parkin, B. A. Gurney, D. R. Wilhoit, and D. Mauri, Phys. Rev. B **43**, 1297 (1991).
[6] J. Fujikata, K. Hayashi, H. Yamamoto, and K. Yamada, J. Magn. Soc. Jpn. **19**, 265 (1995).
[7] J. C. S. Kools, IEEE Trans. Magn. **32**, 3165 (1996).
[8] F. C. Farrow, R. F. Marks, S. Gider, A. C. Marley, and S. S. P. Parkin, J. Appl. Phys. **81**, 986 (1997).
[9] K. Nishioka, S. Gangopadhyay, A. Fujiwara, and M. Parker, IEEE Trans. Magn. **32**, 949 (1995).
[10] B. Dieny, V. Speriosu, S. P. Parkin, P. Baumgart, and D. Wilhoit, J. Appl. Phys. **69**, 4774 (1991).
[11] M. Kiwi, J. Magn. Magn. Mater. **234**, 584 (2001).
[12] W. H. Meiklejohn and C. P. Bean, Phys. Rev. **105**, 904 (1957).
[13] W. H. Meiklejohn, J. Appl. Phys. **33**, 1328 (1962).
[14] L. Néel, Ann. Phys. **2**, 61 (1967).
[15] D. Mauri, H. C. Siegmann, P. S. Bagus, and E. Kay, J. Appl. Phys. **62**, 3047 (1987).
[16] A. P. Malozemoff, J. Appl. Phys. **63**, 3874 (1998); Phys. Rev. B **35**, R3679 (1987).
[17] T. J. Moran and I. K. Schuller, J. Appl. Phys. **79**, 5109 (1996).
[18] N. C. Koon, Phys. Rev. Lett. **78**, 4865 (1997).
[19] T. C. Schulthess and W. H. Butler, Phys. Rev. Lett. **81**, 4516 (1998).
[20] T. C. Schulthess and W. H. Butler, J. Appl. Phys. **85**, 5510 (1999).
[21] U. Nowak, A. Misra, and K. D. Usadel, J. Appl. Phys. **89**, 7269 (2001).
[22] U. Nowak, K. D. Usadel, J. Keller, P. Miltenyi, B. Beschoten, and G. Guntherodt, Phys. Rev. B **66**, 014430 (2002).
[23] A. Misra, U. Nowak, and K. D. Usadel, J. Appl. Phys. **93**, 6593 (2003).
[24] B. Beckmann, U. Nowak, and K. D. Usadel, Phys. Rev. Lett. **91**, 187201 (2003).
[25] M. R. Fitzsimmons, P. Yashar, C. Leighton, I. K. Schuller, J. Nogues, C. F. Majkrzak, and J. A. Dura, Phys. Rev. Lett. **84**, 3986 (2000).
[26] Y. Ijiri, J. A. Borchers, R. W. Erwin, S. H. Lee, P. J. vanderZaag, and R. M. Wolf, Phys. Rev. Lett. **80**, 608 (1998).
[27] H. Zabel, R. Siebrecht, and A. Schreyer, Physica B **276**, 17 (2000).
[28] M. R. Fitzsimmons, S. D. Bader, J. A. Borchers, G. P. Felcher, J. K. Furdyna, A. Hoffmann, J. B. Kortright, I. K. Schuller, T. C. Schulthess, S. K. Sinha, M. F Toney, D. Weller, and S. Wolf, J. Magn. Magn. Mater. **271**, 103 (2004), and references therein.
[29] J. B. Kortright, D. D. Awschalom, J. Stöhr, S. D. Bader, Y. U. Idzerda, S. S. Parkin, and I. K. Schuller, J. Magn. Magn. Mater. **207**, 7 (1999).
[30] H. Ohldag, A. Scholl, F. Nolting, S. Anders, F. U. Hillebrecht, and J. Stöhr, Phys. Rev. Lett. **86**, 2878 (2001).
[31] B. P. Tonner, D. Dunham, T. Droubay, J. Kikuma, and J. Denlinger, J. Electron Spectrosc. Relat. Phenom. **78**, 13 (1996).
[32] Ch. Sauer and W. Zinn, in *Magnetic Multilayers*, edited by L. H. Bennett and R. E. Watson (World Scientific, Singapore, 1993).
[33] T. Shinjo and W. Keune, J. Magn. Magn. Mater. **200**, 598 (1999).
[34] V. E. Kuncser, M. Doi, W. Keune, M. Askin, H. Spies, J. S. Jiang, A. Inomata, and S. D. Bader, Phys. Rev. B **68**, 064416 (2003).
[35] W. A. A. Macedo, B. Sahoo, V. Kuncser, J. Eisenmenger, I. Felner, J. Nogues, K. Liu, W. Keune, and I. K. Schuller, Phys. Rev. B **70**, 224414 (2004).
[36] V. Kuncser, M. Doi, B. Sahoo, F. Stromberg, and W. Keune, J. Appl. Phys. **94**, 3573 (2003).
[37] V. E. Kuncser, F. Stromberg, M. Acet, and W. Keune, J. Appl. Phys. **97**, 63513 (2005)
[38] V. I. Nikolaev, Yu. I. Shcherbina, and S. S. Yakimov, Sov. Phys. JETP **45**, 1277 (1963).
[39] G. Venturini, B. Malaman, G. LeCaër, and D. Fruchart, Phys. Rev. B **35**, 7038 (1987).
[40] G. Venturini, D. Fruchart, J. Hübsch, G. Le Caër, B. Malaman, and B. Roques, J. Phys. F: Met. Phys. **15**, 427 (1985).
[41] G. Le Caër, B. Malaman, G. Venturini, D. Fruchart, and B. Roques, J. Phys. F: Met. Phys. **15**, 1813 (1985).
[42] R. A. Brand, Nucl. Instrum. Methods Phys. Res. B **28**, 398 (1987); the NORMOS program is available from WISSEL GmbH, D-82319 Starnberg, Germany.
[43] U. Gonser, in *Mössbauer Spectroscopy*, Topics in Applied Physics Vol. 5, edited by U. Gonser (Springer, Berlin, 1975) p. 1.
[44] H. D. Pfannes and H. Fischer, Appl. Phys. **13**, 317 (1977).
[45] J. M. Greneche and F. Varret, J. Phys. C **15**, 5333 (1982).
[46] Q. A. Pankhurst and M. R. Gibb, J. Phys.: Condens. Matter **5**, 3275 (1993).
[47] I. S. Grigoriev and E. Z. Meilikhov, *Handbook of Physical Quantities* (CRC Press, Boca Raton, Florida, 1997).